Shock Waves
https://doi.org/10.1007/s00193-018-00889-6

ORIGINAL ARTICLE

Non-uniform ignition behind a reflected shock and its influence on ignition delay measured in a shock tube

C. Huang[1] · **C. Qi**[1] · **Z. Chen**[1,2]

Received: 3 September 2018 / Revised: 7 December 2018 / Accepted: 31 December 2018

Abstract

Accurate measurement of ignition delay in a shock tube is extremely important for developing chemical mechanisms of different fuels. In ideal shock-tube experiments, the test gas behind the reflected shock is expected to ignite uniformly. However, in practical shock-tube experiments, non-uniform ignition occurs due to different factors such as boundary layer growth and boundary layer–reflected shock interaction. Such non-uniform ignition greatly complicates the interpretation of measurements and affects the accuracy of ignition delay measurement. Even without boundary layer and multi-dimensional effects, non-uniform ignition can still happen since the reflected shock itself can induce the spatial gradient of ignition delay. This was first studied numerically by Melguizo-Gavilanes and Bauwens (Shock Waves 23(3):221–231, 2013) using a simplified three-step chemical mechanism. They found that non-uniform ignition can greatly affect the determination of ignition delay in a shock tube. As an extension of Melguizo-Gavilanes and Bauwens' work, in the present study we conduct simulations considering detailed chemistry for two fuels, hydrogen and n-heptane, without and with low-temperature chemistry. Moreover, the detonation development for different mixtures is interpreted through comparing the local sound speed and reaction front propagation speed. The ignition delay recorded at different positions away from the end wall is compared to that in a homogeneous system. A large deviation in ignition delay is observed. The deviation is shown to change linearly with the distance away from the end wall, and a correlation is proposed to accurately describe such deviations.

Keywords Shock tube · Non-uniform ignition · Ignition delay · Detonation development

1 Introduction

The ignition delay measured in shock-tube experiments is popularly used to develop and validate chemical mechanisms [1]. Accurate measurement of ignition delay is extremely important since it is difficult to constrain the uncertainty of chemical models using experimental data with large uncertainty. In ideal shock-tube experiments, the test gas behind the reflected shock should be stationary and uniform, in which homogeneous ignition is expected. However, in practical shock-tube experiments, there are non-ideal behaviors resulting from boundary layer growth and the interaction between boundary layer and reflected shock, which result in non-uniform, inhomogeneous ignition [2]. Such non-uniform ignition can greatly affect the accuracy of ignition delay measurements in a shock tube [3].

In the literature, there are many studies on the ignition behavior behind a reflected shock. For example, Strehlow and coworkers [4, 5] identified three types of ignition behavior in a shock tube. Voevodsky and Soloukhin [6] identified weak and strong ignition regimes based on the second explosion limit of hydrogen–oxygen mixtures. Meyer and Oppenheim [7] showed that the ignition kernels start at a distance away from the shock-reflecting wall in the weak ignition regime. Oran et al. [8, 9] conducted simulations for cases in weak and strong regimes of hydrogen–oxygen–argon mixtures, and they found that the ignition delay at a distance away from the shock-reflecting wall is much smaller than the calculated chemical induction time. Yamashita et al. [10] found that there are ignition positions around the central axis

---

Communicated by A. Higgins.

✉ Z. Chen
cz@pku.edu.cn

[1] CAPT, SKLTCS, College of Engineering, Peking University, Beijing 100871, China

[2] Beijing Innovation Center for Engineering Science and Advanced Technology, Peking University, Beijing 100871, China

of the shock tube and that local ignition can be induced by bifurcated shock waves behind the reflected shock. Grogan and Ihme [2] found that multi-dimensional effects can cause non-uniform ignition and that wall-heat transfer has a strong impact on ignition. Uygun [3], Javed et al. [11], and Ninnemann et al. [12] observed that pre-ignition occurs in shock-tube experiments, which complicates the interpretation of measurements. In the recent study of Tulgestke et al. [13], inhomogeneous ignition was visualized in a shock tube and it was caused by small particle fragmentation after arrival near the end wall.

Most of the studies mentioned above focused on the non-uniform ignition due to the interaction between boundary layer and reflected shock, localized (pre-) ignition kernels, or multi-dimensional effects. Unlike previous studies, this work focuses on non-uniform ignition due to the fact that the test gas is consecutively compressed by the reflected shock. Since the mixture closer to the end wall is compressed earlier by the reflected shock, it needs a shorter time for ignition to happen. Figure 1 shows the approximate spatial distribution of the time required for ignition to happen, $\tau_\mathrm{i}(x) \approx \tau_\mathrm{i}^0 - (x_\mathrm{shock} - x)/u_\mathrm{shock}$, at the moment that the reflected shock arrives at $x = x_\mathrm{shock}$. The mixture just after the reflected shock (i.e., $x = x_\mathrm{shock}$) has the longest ignition delay of τ_i^0. For the mixture close to the end wall (i.e., $x = 0$), the time required for ignition to happen is approximately equal to $\tau_\mathrm{i}^0 - x_\mathrm{shock}/u_\mathrm{shock}$. Therefore, the reflected shock itself can induce the gradient of ignition delay. According to the reactivity gradient mechanism of Zel'dovich [14] and the SWACER mechanism of Lee et al. [15], detonation may develop due to the gradient of ignition delay. Such kind of shock-induced detonation was studied by different groups in experiments (e.g., [16]). However, its influence on the determination of ignition delay in a shock tube was only first studied by Melguizo-Gavilanes and Bauwens [17] through numerical simulations using a simplified three-step chain-branching kinetic scheme. In their simulation results, detonation development due to non-uniform ignition after the reflected shock was observed. They concluded that the spatial non-uniformities result in the ignition delays measured in shock-tube experiments being different from that in a homogeneous isochoric (constant UV) or isobaric (constant HP) reactor [17].

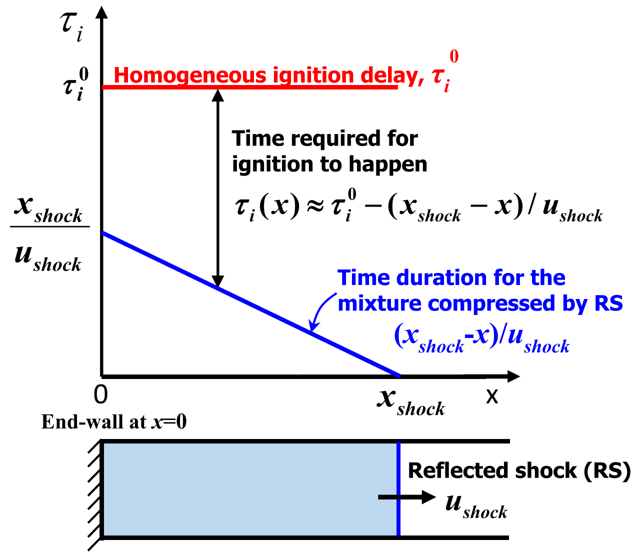

Fig. 1 Approximate spatial distribution of the time required for ignition to happen, $\tau_\mathrm{i}(x) \approx \tau_\mathrm{i}^0 - (x_\mathrm{shock} - x)/u_\mathrm{shock}$, at the moment that the reflected shock arrives at $x = x_\mathrm{shock}$. The speed of reflected shock is u_shock, and the homogeneous ignition delay is τ_i^0 for the mixture immediately after the reflected shock (i.e., at $x = x_\mathrm{shock}$)

As an extension of Melguizo-Gavilanes and Bauwens's work [17], here we conduct simulations considering detailed chemistry for two fuels, hydrogen and n-heptane. n-Heptane is considered here since it has two-stage ignition when the temperature is within the negative temperature coefficient (NTC) region. The two-stage ignition cannot be reproduced by the three-step chemistry used in [17]. Moreover, the ratio of the local sound speed to reaction front propagation speed is derived, and it is used to interpret the detonation development after the reflected shock. Besides, a correlation is proposed to describe the deviation in ignition delay based on the pressure history recorded at different positions in a shock tube with that for a homogeneous isochoric process. This was not reported in [17].

Similar to the work of Melguizo-Gavilanes and Bauwens [17], the multi-dimensional effects (e.g., shock–boundary interactions [18] and complicated wall-bounded flows [19]) are deliberately avoided since we focus on the non-uniform ignition caused by the propagation of the reflected shock itself. Therefore, one-dimensional simulations are conducted here. First, the mechanism for detonation development is analyzed. Then, ignition delay recorded at different positions away from the end wall is obtained and compared to that in a homogeneous system. The deviation in ignition delay is analyzed and interpreted. Finally, a correlation is derived from theoretical analysis, and it can accurately describe the deviation between the measured ignition delay and that in a corresponding homogeneous system.

2 Numerical model and specifications

A one-dimensional simulation is conducted to study the transient ignition and detonation development process after a reflected shock. The length of the computational domain is long enough to ensure that ignition starts near the end wall during the propagation of the reflected shock (i.e., the computational domain length is larger than the speed of reflected shock multiplying the ignition delay) and that the interaction between the reflected shock and contact surface is artificially prevented. Initially, the incident shock located at some distance (e.g., 15 cm) from the end wall on the left side. Then, it propagates to the left side and it reflects off the adiabatic end wall, which is located at the left boundary, $x = 0$ cm, as shown in Fig. 1. The right side is a non-reflecting boundary condition. The end wall is considered to be adiabatic rather than at a fixed wall temperature, which simplifies the process of shock reflection on the wall. In practical shock-tube experiments, there is heat loss on the end wall and this deserves further study.

The one-dimensional transient shock propagation, autoignition, and detonation development processes are simulated using the in-house code A-SURF [20–22]. A-SURF solves the following conservation equations of mass, momentum, species, and total energy for one-dimensional, adiabatic, multi-component, reacting compressible flows [20–22]:

$$\frac{\partial U}{\partial t} + \frac{\partial F(U)}{\partial x} = F_{\mathrm{v}}(U) + S_{\mathrm{R}} \tag{1}$$

where t and x are the temporal and spatial coordinates, respectively. The vectors U, $F(U)$, $G(U)$, $F_{\mathrm{v}}(U)$, and S_{R} are defined as:

$$U = \begin{pmatrix} \rho Y_1 \\ \rho Y_2 \\ \vdots \\ \rho Y_n \\ \rho u \\ E \end{pmatrix}, F(U) = \begin{pmatrix} \rho u Y_1 \\ \rho u Y_2 \\ \vdots \\ \rho u Y_n \\ \rho u^2 + P \\ (E+P)u \end{pmatrix}, G(U) = \begin{pmatrix} \rho u Y_1 \\ \rho u Y_2 \\ \vdots \\ \rho u Y_n \\ \rho u^2 \\ (E+P)u \end{pmatrix},$$
$$F_{\mathrm{v}}(U) = \begin{pmatrix} -(\rho Y_1 V_1')_x \\ -(\rho Y_2 V_2')_x \\ \vdots \\ -(\rho Y_n V_n')_x \\ (\tau)_x \\ q_x + \Phi \end{pmatrix}, S_{\mathrm{R}} = \begin{pmatrix} \omega_1 \\ \omega_2 \\ \vdots \\ \omega_n \\ 0 \\ 0 \end{pmatrix} \tag{2}$$

where ρ is the density, u the flow velocity, Y_k the mass fraction of species k, and E the total energy per unit mass. The subscript x in $F_{\mathrm{v}}(U)$ stands for the partial derivative with respect to x.

In the species conservation equations, ω_k is the production rate of species k, which is calculated using the CHEMKIN package [23]. The mixture-averaged formula is used to calculate the diffusion velocity of the kth species, V_k', which is composed of three parts:

$$V_k' = V_{k,Y}' + V_{k,\mathrm{T}}' + V_{k,\mathrm{C}}' \tag{3}$$

where $V_{k,Y}'$, $V_{k,\mathrm{T}}'$, and $V_{k,\mathrm{C}}'$ are the ordinary diffusion velocity, thermal diffusion velocity, and the correction velocity, respectively. The correction velocity $V_{k,\mathrm{C}}'$ is included to ensure the compatibility of the species and mass conservation equations [24].

In the momentum equation, P is the pressure and the viscous stresses, τ, is modeled as

$$\tau = 2\mu\frac{\partial u}{\partial x} - \frac{2}{3}\mu\frac{\partial u}{\partial x} \tag{4}$$

where μ is the dynamic viscosity of the mixture.

In the energy conservation equation, E is the total energy. The heat flux q includes a heat diffusion term expressed by Fourier's law and a second term associated with the diffusion of species with different enthalpies.

$$q = \left[\lambda\frac{\partial T}{\partial x} - \rho\sum_{k=1}^{n}(h_k Y_k V_k')\right] \tag{5}$$

where λ is the thermal conductivity of the mixture. In the energy equation, the viscous dissipation rate is

$$\Phi = \mu\left\{2\left(\frac{\partial u}{\partial x}\right)^2 - \frac{2}{3}\left[\frac{\partial u}{\partial x}\right]^2\right\} + u\frac{\partial \tau}{\partial x} \tag{6}$$

The pressure can be calculated from the ideal gas law

$$P = \rho RT/\bar{M} \tag{7}$$

where $R = 8.314$ J/(mol K) is the universal gas constant and $\bar{M}$ is the mean molecular weight.

The CHEMKIN and TRANSPORT packages [23, 24] are used to calculate the thermodynamic and transport properties in (2–7). The finite volume method is used to solve the conservation equations. The time evolution of the stiff reaction term is separated from that of the convection and diffusion terms by using the Strang splitting fractional-step procedure [25]. In the first and third half fractional steps, the conservation equations for non-reactive flow are solved. The temporal integration, convective flux, and diffusive flux are calculated, respectively, using the Runge–Kutta, MUSCL-Hancock (with MINBEE flux limiter) [26], and central difference schemes. In the second fractional step, the chemistry is solved using the semi-implicit integration method [27]. A-SURF has been successfully used in previous studies on flame propagation, end-gas autoignition, and detonation development (e.g., [28–33]). The details on numerical methods and code validations can be found in Refs. [20–22] and thereby are not repeated here.

Two mixtures are considered here: One is stoichiometric hydrogen–oxygen with different amounts of argon dilution, and the other is stoichiometric n-heptane–oxygen with nitrogen dilution. The detailed chemistry for hydrogen [34] (with 10 species and 21 elementary reactions) and the skeletal mechanism for n-heptane with low-temperature chemistry [35] (with 44 species and 112 elementary reactions) are used in the simulations. In order to accurately and efficiently resolve the propagation of shock wave, autoignition, and detonation, a dynamically adaptive mesh refinement strategy is adopted. Mesh refinement and coarsening are conducted based on the local temperature and pressure gradients. The base mesh size before refinement is 4.096 mm. After 10 levels of mesh refinement, the finest mesh size is 4 μm. The corresponding time step is 0.15 ns. The shortest induction length for detonations observed in this study is around 100 μm. Therefore, enough resolution is ensured for simulating detonation development and propagation. Numerical convergence has been checked and ensured by further decreasing the time step and mesh size in simulations.

It is noted that in our simulations, the governing equations and initialization are different from those in of Melguizo-Gavilanes and Bauwens [17]. Here, we solve the traditional conservation equations for compressible reactive flow based on Eulerian rather than Lagrangian coordinates. Initially, the shock is not on the end wall. The incident shock is initially located at some distance from the end wall. During time evolution, the incident shock propagates toward the end wall and reflects off it. As the reflected shock moves away from the end wall, the region between the reflected shock and the end wall becomes larger, leading to unavoidable resolution problems initially as a few grid points will be present in the region of interest. However, this does not have a strong effect on the simulation results since a small grid size of 4 μm is used in our simulation. For a reflected shock propagating at a speed on the order of 1000 m/s, it takes only 4 ns to pass a grid. Such a short time has little effect on the ignition process which has the timescale on the order of 1–1000 μs. In addition, numerical tests with the smallest grid size of 1 μm indicated that grid convergence is achieved for a grid size of 4 μm. Therefore, here we do not need to handle the singular nature of the initial conditions as in [17].

3 Results and discussion

3.1 Hydrogen–oxygen–argon mixture

3.1.1 Detonation development

First, we investigate the detonation development process after the reflected shock for stoichiometric hydrogen–oxygen mixtures with different amounts of argon dilution. Figure 2 shows the temporal evolution of temperature and pressure distributions during the autoignition after a reflected shock in stoichiometric H_2–O_2 with 40% vol. Ar dilution. The temperature and pressure after the reflected shock are $T_S = 1032.3$ K and $P_S = 1.38$ atm, respectively. The incident shock Mach number is 2.36, and its pressure ratio is 5.69. The corresponding temperature and pressure after the incident shock are 649.45 K and 0.376 atm, respectively. Timing starts when the reflected shock leaves the end wall at $x = 0$ cm. At $t = 81.1$ μs (line #2 in Fig. 2), autoignition starts near the end wall and the reaction front propagates to the right side. At $t = 83.7$ μs (line #3), a shock is developed due to the coherent coupling between ignition and the pressure wave [36, 37]. Eventually, a detonation develops and it propagates to the right side at a speed of 1890 m/s (lines #4–6), which is very close to the CJ speed of 1928 m/s. Since the leading reflected shock propagates slower than the detonation, the detonation can eventually catch up and merge with the reflected shock. This process is schematically summarized in Fig. 3.

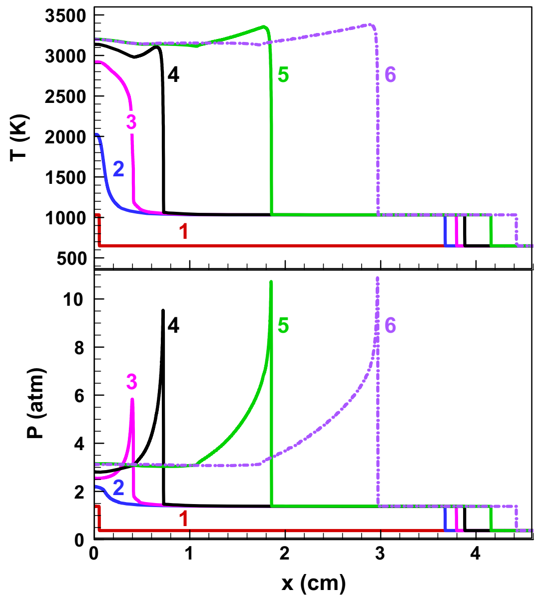

Fig. 2 Temporal evolution of temperature and pressure distributions for stoichiometric H_2–O_2 with 40% vol. Ar dilution. The temperature and pressure after the reflected shock are $T_S = 1032.3$ K and $P_S = 1.38$ atm, respectively. The time sequence from line #1 to #6 is $t = 1.1$, 81.1, 83.7, 85.4, 91.7, and 97.6 μs (at $t = 0$ μs, the reflected shock leaves the end wall at $x = 0$ cm)

The above detonation development process can be explained by the reactivity gradient mechanism [14]. According to Gu et al. [38], detonation development can be characterized by the non-dimensional parameter, ξ, which represents the ratio of local sound speed, a, to reaction front propagation speed, u_f. The reaction front propagation speed is equal to the inverse of the ignition gradient [14]:

$$u_f = \left(\frac{d\tau_i(x)}{dx} \right)^{-1} \tag{8}$$

in which $\tau_i(x)$ is the spatial distribution of ignition delay. Approximately we can assume that autoignition happens independently at each point after the reflected shock and thereby $\tau_i(x) \approx \tau_i^0 - (x_{shock} - x)/u_{shock}$ as indicated in Fig. 1. Therefore, we have $u_f = 1/(d\tau_i(x)/dx) \approx u_{shock}$. It is noted that this is just a first-order approximation since autoignition at

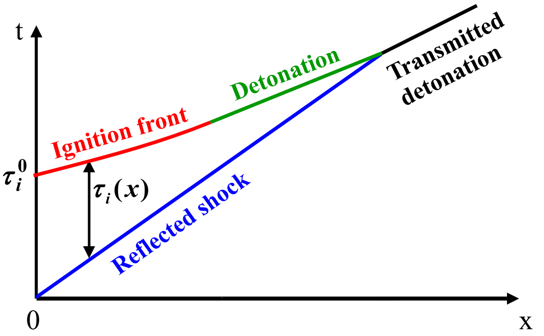

Fig. 3 Schematic of trajectories of reflected shock, ignition front, and detonation waves

each point is not an independently isochoric process, which will be shown later. In fact, the reaction front does not propagate at exactly the same speed as the reflected shock. But such an approximation does help to explain the detonation development. Therefore, approximately we have

$$\xi = \frac{a}{u_{\mathrm{f}}} \approx \frac{a}{u_{\mathrm{shock}}} = \frac{1}{M_{\mathrm{shock}}} \tag{9}$$

where M_{shock} is the Mach number of the reflected shock. It is noted that the sound speed behind the reflected shock, rather than the one before the reflected shock, is used in (9). Over the course of detonation development, the reaction front will be steep and evolves into a detonation wave that eventually overtakes the reflected shock. Thus, the approximation of $u_{\mathrm{f}} \approx u_{\mathrm{shock}}$ is only used here to explain the detonation development, and it cannot be used later in (11). After a simple derivation based on the relationships for incident and reflected shock waves [39], we have

$$\xi \approx \frac{1}{M_{\mathrm{shock}}} = \left[\frac{\frac{\gamma+1}{2}\left[\frac{(3\gamma-1)k-(\gamma-1)}{\gamma+1+k(\gamma-1)} + \frac{\gamma-1}{\gamma+1}\right] - \frac{\gamma-1}{2}}{1 + \frac{\gamma^2-1}{4\gamma}\left[\frac{(3\gamma-1)k-(\gamma-1)}{\gamma+1+k(\gamma-1)} + \frac{\gamma-1}{\gamma+1}\right]} \right] \tag{10}$$

in which γ is the heat capacity ratio and k is the pressure ratio of the incident shock. Calculation results based on (10) are shown in Fig. 4. It is observed that $1 < \xi < 2.5$. This means that the reaction–autoignition front propagates at a speed close to the local sound speed. Therefore, chemical reaction can coherently couple with the pressure wave [38]. The mutual reinforcement between chemical reaction and the pressure wave eventually leads to the detonation development shown in Fig. 2.

Similar results of detonation development are obtained for stoichiometric H_2–O_2 with 70% vol. argon dilution. With the increase in argon dilution, detonation development becomes slower due to lower heat release rate and longer excitation time (which is defined as the time interval for heat release [38]). When argon dilution reaches 90% vol., Fig. 5 shows that a detonation cannot be developed. The reaction front (defined as the location of maximum heat release rate) propagates at the speed in the range of 500–900 m/s, which is much lower than the CJ speed of 1332 m/s. Moreover, the peak pressure, around 3.74 atm, is much lower than the pressure at the corresponding von Neumann spike, 6.98 atm. (It

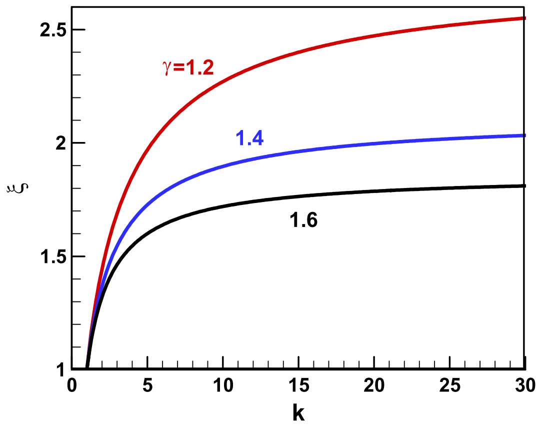

Fig. 4 Change of ξ with k for different values of γ as predicted by (10)

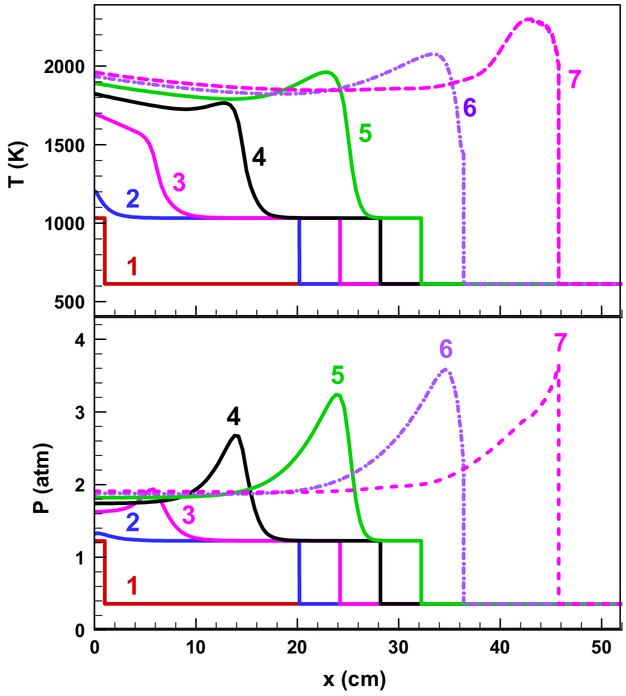

Fig. 5 Temporal evolution of temperature and pressure distributions for stoichiometric H_2–O_2 with 90% vol. Ar dilution. The temperature and pressure after the reflected shock are $T_S = 1032.2$ K and $P_S = 1.23$ atm, respectively. The time sequence from line #1 to #7 is $t = 20, 500, 600, 700, 800, 900, 1000$ μs

is based on the conditions of 1032.2 K and 1.23 atm behind the reflected shock.)

3.1.2 The ignition delay time

To investigate the autoignition process after the reflected shock, we track the flow particles at different initial locations [29]. The position of a flow particle is first updated by its current flow speed multiplying the time step size of $\Delta t = 0.15$ ns which is fixed in the simulation; then, the thermal states and flow speed of this particle are obtained from linear interpolation of corresponding values at its two neighboring grids [29]. Figure 6 shows the results for the case shown in Fig. 2. It is observed that for the particle near the reflecting wall, $X_0 = 1$ mm, the autoignition process is neither isochoric nor isobaric. The particle first experiences expansion during its autoignition process. Then, it is compressed due to autoignition in its neighboring particles. For the particle initially at $X_0 = 2$ mm, during its autoignition process, it is compressed by the autoignition of particles on its left side (i.e., $X_0 < 2$ mm). For particles initially at $X_0 = 5$ and 15 mm, they go through the typical detonation process containing the compression by a shock wave and autoignition afterward. Therefore, the autoignition at each point after the reflected shock is not an independently isochoric or isobaric process, and it is affected by expansion or compression due to its neighbor.

To mimic the ignition delay measurement in a shock tube, in simulations we record the pressure history at different positions away from the end wall. The results for stoichiometric H_2–O_2 with 40% and 90% vol. argon dilution are shown in Fig. 7. It is noted that timing starts when the reflected shock passes the recording position. For comparison, the results for homogeneous ignition at constant volume are also plotted in Fig. 7. The ignition delay at a certain recording position X_P is denoted as $\tau_i(X_P)$, and it is defined as the time interval between passage of the reflected shock and the maximum pressure rise rate. For the constant-volume and constant-pressure homogeneous ignition processes, their ignition delay τ_i^0 is defined as the time of maximum pressure and temperature rise rate, respectively. It is noted that—as suggested by one of the anonymous reviewers—while the various definitions often coincide for highly exothermic events at low dilution levels [40], there can be noticeable differences between different ignition time markers for more dilute conditions.

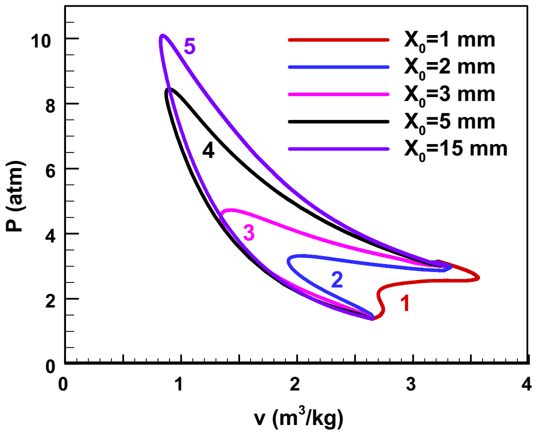

Fig. 6 The pressure versus specific volume, P–v, diagrams for particles at different initial positions of $X_0 = 1$–15 mm for the case shown in Fig. 2

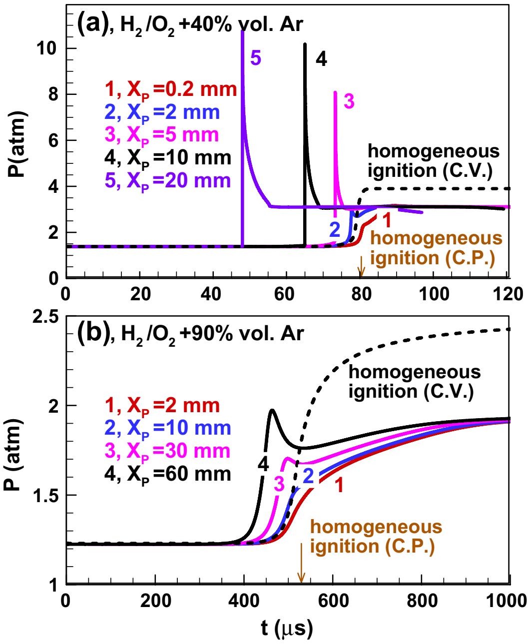

Fig. 7 Temporal evolution of pressure recorded at different positions, *XP*. The dashed lines show the results for homogeneous ignition at constant volume (C.V.)

Figure 7a shows that the ignition delay decreases when the recording position moves away from the end wall (i.e., increasing X_P). Similar observation was found in previous simulation based on three-step chemistry [17]. This is due to the non-uniform ignition and detonation development as shown in Fig. 2. It is noticed that the ignition delay recorded near the end wall, $X_P = 0.2$ mm, is slightly longer than that for a constant-volume homogeneous ignition process. This is due to the expansion shown in Fig. 6. When argon dilution is increased to 90% vol., Fig. 7b indicates that the ignition delay recorded at different positions is close to that for a constant-volume homogeneous ignition process. Therefore, from Fig. 7, we conclude that due to non-uniform ignition and detonation development, the ignition delay decreases as the recording position moves away from the end wall, and that such differences can be reduced by increasing argon dilution. In [17], heat release was changed, and this

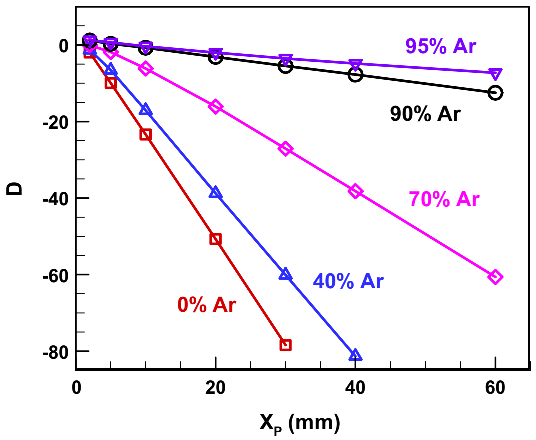

Fig. 8 The deviation, $D=\tau_{\mathrm{i}}(X_{\mathrm{P}})/\tau_{\mathrm{i}}^{0}-1$, for ignition delay recorded at different positions for stoichiometric H_2–O_2 with different amounts of Ar dilution. The homogenous ignition delay at constant volume is $\tau_{\mathrm{i}}^{0}=48.2$, 78.4, 157.6, 523.2, and 1055 µs, respectively, for 0, 40, 70, 90, and 95% Ar dilution

procedure is equivalent to changing the dilution ratio. The present results based on detailed chemistry are consistent with those in [17] based on simplified three-step chemistry.

Figure 8 depicts the deviation for ignition delay recorded at different positions. The derivation is defined as $D=\tau_{\mathrm{i}}(X_{\mathrm{P}})/\tau_{\mathrm{i}}^{0}-1$, where $\tau_{\mathrm{i}}(X_{\mathrm{P}})$ is the ignition delay recorded at $x=X_{\mathrm{P}}$ and τ_{i}^{0} is the ignition delay of the constant-volume (isochoric) homogeneous ignition process. For the derivation $D=\tau_{\mathrm{i}}(X_{\mathrm{P}})/\tau_{\mathrm{i}}^{0}-1$ and the values of D and τ_{i}^{0} shown in Fig. 8, $\tau_{\mathrm{i}}(X_{\mathrm{P}})$ can be readily evaluated, and therefore it is not plotted in another figure. Figure 8 shows that deviation changes linearly with the distance away from the end wall and that the absolute value of deviation decreases with the increase in argon dilution. A similar observation was found in [17]. Such observations can be explained by the following analysis. According to the definition, the ignition delay at $x=X_{\mathrm{P}}$ is equal to the difference between the time elapsed by the reflected shock and reaction front to arrive at this recording position. At early times immediately after shock reflection on the end wall, the reaction front speed u_{f} is highly transient. After the transient process, the speeds of the reflected shock u_{shock} and reaction front u_{f} can be approximately assumed to remain constant and we have the following expression for the deviation:

$$D=\frac{1}{\tau_{i}^{0}}\left(\frac{X_{\mathrm{P}}}{u_{\mathrm{shock}}}-\frac{X_{\mathrm{P}}}{u_{\mathrm{f}}}+\Delta t\right) \qquad (11)$$

in which Δt is the difference between τ_{i}^{0} and the ignition delay at the reflecting wall (i.e., $X_{\mathrm{P}}=0$). In simulations, the reaction front x_{f} is defined as the position with the local maximum pressure gradient and a nonzero reaction rate (otherwise it occurs at the shock position), and the reaction front speed is obtained from numerical differentiation according to $u_{\mathrm{f}}=\mathrm{d}x_{\mathrm{f}}/\mathrm{d}t$. According to the results in Fig. 7, $\Delta t/\tau_{\mathrm{i}}^{0}$ is close to zero (around 2%) and negligible for H_2–O_2–Ar mixture. Equation (11) indicates that the deviation changes linearly with the distance away from the end wall, X_{P}. This is consistent with the trend shown in Fig. 8. As shown in Fig. 7, the ignition delay τ_{i}^{0} increases greatly with argon dilution. Therefore, according to (11), the absolute value of deviation should decrease with the increase in argon dilution as shown in Fig. 8. It is noted that argon dilution also changes the overall ratio of specific heat capacities and thereby the compressibility of the mixture. However, the influence of dilution on the deviation is mainly due to its change in the ignition delay rather than the compressibility of the mixture. Figure 8 indicates that at very high dilution levels (e.g., above 95% argon dilution), the gas dynamic effects of ignition (the theme of the present manuscript) are minimal and can be neglected. Besides, the pressure measurements in most shock-tube tests are not conducted at large distances away from the end wall and in many cases they are done directly from the end wall. Therefore, the gas dynamic effects are diminished according to Fig. 8 and (11).

Figure 9 shows that the deviation given by (11) agrees very well with that from calculation. The good agreement also indicates that the approximation of constant u_{shock} and u_{f} is reasonable. In shock-tube experiments, if the speeds of reflected shock u_{shock} and reaction front u_{f} can be measured at different positions, (11) can be used to correct the ignition delay recorded at different positions away from the end wall. In shock-tube experiments, the reflected shock speed u_{shock} might be accurately measured or found from normal shock relations. The speed of reaction front u_{f} can be obtained from the maximum pressure rise rate in pressure measurements at different positions.

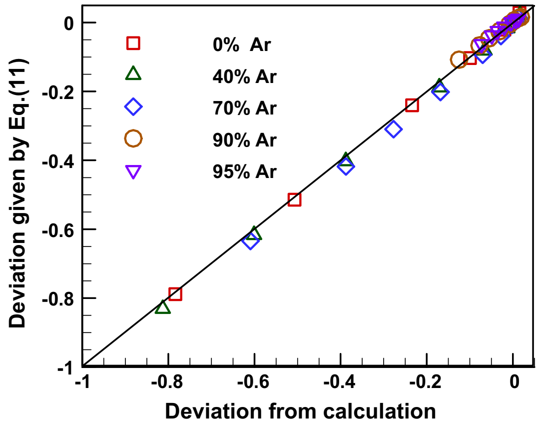

Fig. 9 Comparison between the deviation given by (11) and that from calculation for stoichiometric H_2–O_2 with different amounts of Ar dilution

3.2 n-Heptane–oxygen–nitrogen mixture

In this subsection, we consider n-heptane, which has low-temperature chemistry and is one of the main components of the Primary Reference Fuel (PRF) for gasoline. Figure 10 shows the temporal evolution of temperature and pressure distributions during the autoignition after a reflected shock in stoichiometric n-heptane–air mixture. The temperature and pressure after the reflected shock, $T_S = 787.2$ K and $P_S = 8.61$ atm, are within the NTC region. Therefore, as shown later, two-stage autoignition happens in the mixture after the reflected shock. Compared to the H_2–O_2–Ar mixture considered in Sect. 3.1, the nC_7H_{16}–air mixture has much longer ignition delay. Figure 10 shows that ignition starts near the end wall around $t = 5442$ μs (line #2). Due to the reactivity gradient mechanism explained before, detonation development (lines #4–#7 in Fig. 10) is also observed for nC_7H_{16}–air mixture after the reflected shock.

Figure 11 shows the pressure history recorded at different positions away from the end wall. It is noted that, unlike H_2–O_2–Ar mixture whose homogenous ignition delay at constant pressure is nearly the same as that at constant volume (see Fig. 7), Fig. 11 shows that there is a large difference between C.V. and C.P. ignition delay times for nC_7H_{16}–air. This is due to the fact that the influence of pressure on ignition delay is much stronger for of nC_7H_{16}–air than for H_2–O_2–Ar mixtures at the conditions considered in this work. For the case within the NTC region, Fig. 11a indicates that two-stage heat release occurs. As mentioned before, the particle near the end wall, $X_P = 2$ mm, follows an expansion process during its autoignition. Therefore, its ignition delay is much longer than that for the homogeneous ignition at constant volume. When the temperature after the reflected shock is above the NTC region, Fig. 11b shows that the ignition delay recorded near the end wall, $X_P = 2$ mm, is between those for the homogeneous ignition at constant volume and at constant pressure. At higher temperature T_S, the heat release becomes faster and thereby the influence of expansion becomes weaker. Similar to the conclusion drawn for H_2–O_2–Ar, the results for nC_7H_{16}–air also indicate that the autoignition process after the reflected shock is neither isochoric nor isobaric and that due to non-uniform ignition, the ignition delay decreases as the recording position moves away from the end wall.

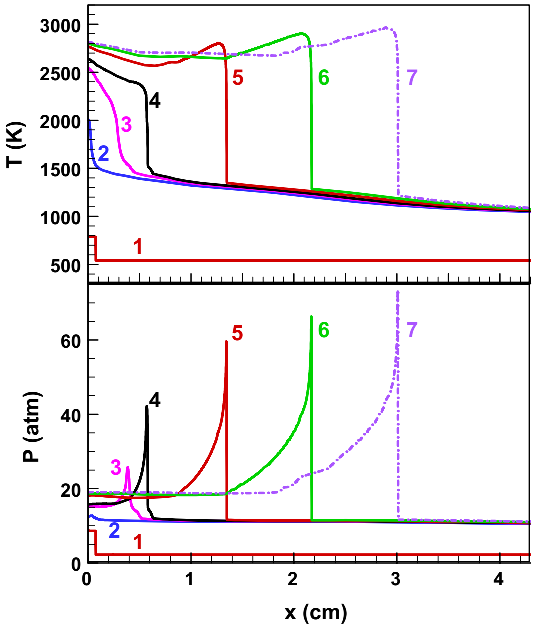

Fig. 10 Temporal evolution of temperature and pressure distributions for stoichiometric nC_7H_{16}/air. The temperature and pressure after the reflected shock are $T_S = 787.2$ K and $P_S = 8.61$ atm, respectively. The time sequence from line #1 to #7 is $t = 2$, 5442, 5447, 5449, 5454, 5459, and 5464 μs (at $t = 0$ μs, the reflected shock leaves the end wall at $x = 0$ cm)

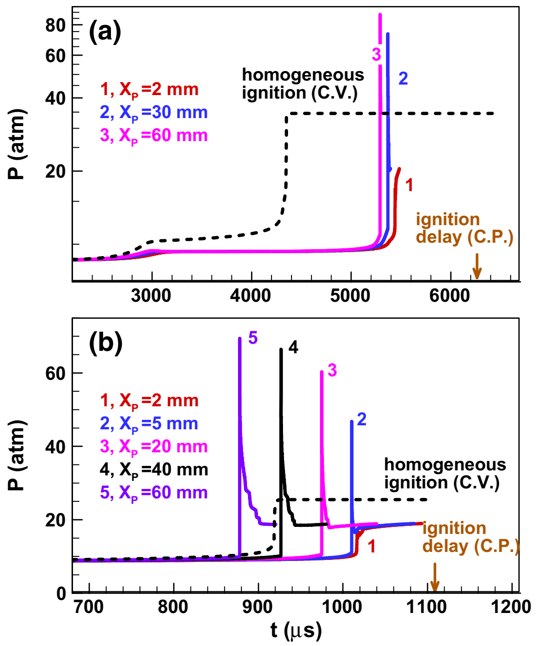

Fig. 11 Temporal evolution of pressure recorded at different positions, X_P, for stoichiometric nC_7H_{16}/air. The temperature and pressure after the reflected shock are **a** $T_S = 787.2$ K and $P_S = 8.61$ atm; **b** $T_S = 1124.2$ K and $P_S = 8.62$ atm. The dashed lines shows the results for homogeneous ignition at constant volume (C.V.)

Figure 12 shows the deviation for ignition delay recorded at different positions for stoichiometric nC_7H_{16}–O_2 with different amounts of N_2 dilution. The results are consistent with those for H_2–O_2–Ar. It is seen that the deviation changes linearly with X_P and that the absolute value of deviation decreases with the increase in nitrogen dilution. Besides, due to the expansion process before ignition, the deviation near the end wall is positive, indicating the ignition delay recorded near the end wall in the shock tube is greater than that in the constant-volume homogeneous system. Again, such deviation can be accurately

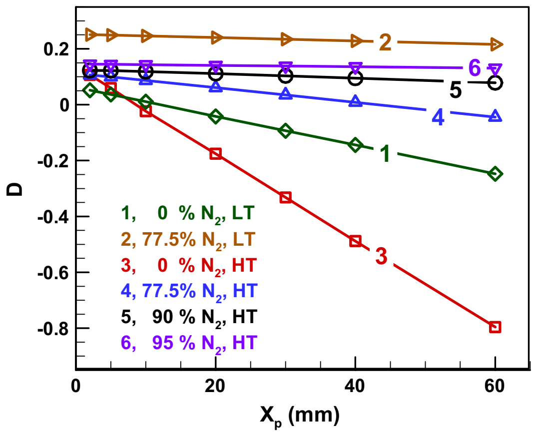

Fig. 12 The deviation, $D=\tau_i(X_P)/\tau_i^0-1$, for ignition delay recorded at different positions for stoichiometric nC_7H_{16}–O_2 with different amounts of N_2 dilution. LT (HT) corresponds to the case that the temperature after the reflected shock is around 786 K (1124 K) and is within (above) the NTC region. The deviation for ignition delay recorded at different positions for stoichiometric H_2–O_2 with different amounts of Ar dilution. The homogenous ignition delay at constant volume is $\tau_i^0=782.0$, 4250.0, 219.3, 918.9, 2312.0, and 5570.0 μs, respectively, for case 1, 2, 3, 4, 5, and 6

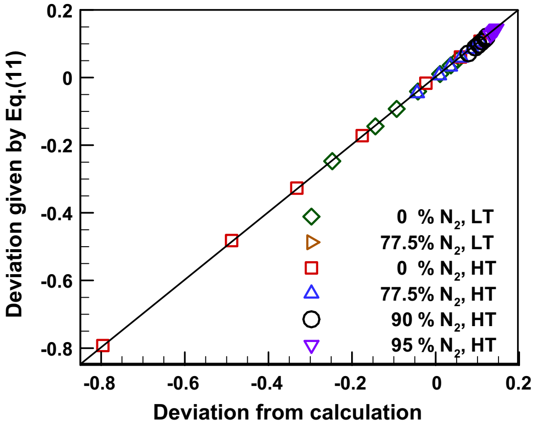

Fig. 13 Comparison between the deviation given by (11) and that from calculation for stoichiometric nC_7H_{16}–O_2 with different amounts of N_2 dilution

given by (11) for nC_7H_{16}–O_2–N_2 mixtures, which is demonstrated in Fig. 13.

Besides n-heptane, we also studied dimethyl ether with low-temperature chemistry. Similar results were obtained for dimethyl ether–air.

4 Conclusions

Numerical simulations were conducted to investigate the non-uniform ignition and detonation development after a reflected shock. This problem was first studied by Melguizo-Gavilanes and Bauwens [17] using a simplified three-step chain-branching kinetic scheme. As an extension of work in [17], here detailed chemistry is considered in simulations. Two fuels, hydrogen and n-heptane, without and with low-temperature chemistry were studied. Similar to results in [17] based on three-step chemistry, the present results based on detailed chemistry indicate that the autoignition at each point after the reflected shock is not an independently isochoric or isobaric process, and it is affected by expansion or compression due to its neighbor. Therefore, the constant-volume or constant-pressure assumption is not appropriate for describing the ignition process in a shock tube, especially for mixtures without high dilution. Unlike the previous work in [17], the ratio of the local sound speed to reaction front propagation speed is derived and it is used together with the reactivity gradient mechanism of Zel'dovich to interpret the detonation development after the reflected shock. Moreover, a correlation is proposed to accurately describe the deviation in ignition delay based on the pressure history recorded at different positions in a shock tube with that for a homogeneous isochoric process. This correlation might be used to correct the ignition delay recorded at different positions away from the end wall if the speeds of the reflected shock and reaction front can be measured in experiments.

It is noted that one-dimensional simulations are conducted here to deliberately avoid the multi-dimensional effects and to focus on the non-uniform ignition caused by the propagation of the reflected shock itself. However, in shock-tube experiments, multi-dimensional effects always exist. Therefore, further work is needed to study the combination of multi-dimensional effects and non-uniform ignition due to the propagation of the reflected shock.

It is also noted that modern ignition delay time measurements in shock tubes are performed considering the sensitivity with dilution level and distance from the end wall [41, 42]. Major shock-tube groups perform their measurements within 1–2 cm from the end wall, and in most cases ignition measurements for dilution levels less than about 95% are done at the end wall and not the sidewall. Therefore, the non-uniform ignition effects can be minimized in modern ignition delay time measurements using shock tubes.

Acknowledgements This work was supported by the National Natural Science Foundation of China (Nos. 91741126 and 91541204). We appreciate helpful discussion with Shengkai Wang at Stanford University and Yuan Wang at Peking University. Part of the simulation was conducted on the High Performance Computing Platform of the Center for Life Science. We thank the editor for improving the English.

References

1. Hanson, R.K., Davidson, D.F.: Recent advances in laser absorption and shock tube methods for studies of combustion chemistry.

Prog. Energy Combust. Sci. **44**(5), 103–114 (2014). https://doi.org/10.1016/j.pecs.2014.05.001

2. Grogan, K.P., Ihme, M.: Weak and strong ignition of hydrogen/oxygen mixtures in shock-tube systems. Proc. Combust. Inst. **35**(2), 2181–2189 (2015). https://doi.org/10.1016/j.proci.2014.07.074
3. Uygun, Y., Ishihara, S., Olivier, H.: A high pressure ignition delay time study of 2-methylfuran and tetrahydrofuran in shock tubes. Combust. Flame **161**(10), 2519–2530 (2014). https://doi.org/10.1016/j.combustflame.2014.04.004
4. Strehlow, R.A., Cohen, A.: Initiation of detonation. J. Phys. Fluids **5**(1), 97–101 (1962). https://doi.org/10.1063/1.1706497
5. Gilbert, R.B., Strehlow, R.A.: Theory of detonation initiation behind reflected shock waves. AIAA **4**(10), 1777–1783 (1966). https://doi.org/10.2514/3.3777
6. Voevodsky, V.V., Soloukhin, R.I.: On the mechanism and explosion limits of hydrogen-oxygen chain self-ignition in shock waves. Symp. (Int.) Combust. **10**(1), 279–283 (1965). https://doi.org/10.1016/S0082-0784(65)80173-4
7. Meyer, J.W., Oppenheim, A.K.: On the shock-induced ignition of explosive gases. Symp. (Int.) Combust. **13**(1), 1153–1164 (1971). https://doi.org/10.1016/S0082-0784(71)80112-1
8. Oran, E.S., Young, T.R., Boris, J.P., Cohen, A.: Weak and strong ignition. I. Numerical simulations of shock tube experiments. Combust. Flame **48**(2), 135–148 (1982). https://doi.org/10.1016/0010-2180(82)90123-7
9. Oran, E.S., Boris, J.P.: Weak and strong ignition. II. Sensitivity of the hydrogen/oxygen system. Combust. Flame **48**(82), 149–161 (1982). https://doi.org/10.1016/0010-2180(82)90124-9
10. Yamashita, H., Kasahara, J., Sugiyama, Y., Matsuo, A.: Visualization study of ignition modes behind bifurcated-reflected shock waves. Combust. Flame **159**(9), 2954–2966 (2012). https://doi.org/10.1016/j.combustflame.2012.05.009
11. Javed, T., Badra, J., Jaasim, M., Es-Sebbar, E., Labastida, M.F., Chung, S.H., Im, H.G., Farooq, A.: Shock tube ignition delay data affected by localized ignition phenomena. Combust. Sci. Technol. **189**(7), 1138–1161 (2017). https://doi.org/10.1080/00102202.2016.1272599
12. Ninnemann, E., Koroglu, B., Pryor, O., Barak, S., Nash, L., Loparo, Z., Sosa, J., Ahmed, K., Vasu, S.: New insights into the shock tube ignition of H_2/O_2 at low to moderate temperatures using high-speed end-wall imaging. Combust. Flame **187**, 11–21 (2018). https://doi.org/10.1016/j.combustflame.2017.08.021
13. Tulgestke, A.M., Johnson, S.E., Davidson, D.F., Hanson, R.K.: High-speed imaging of inhomogeneous ignition in a shock tube. Shock Waves **28**, 1089–1095 (2018). https://doi.org/10.1007/s00193-018-0824-2
14. Zeldovich, Y.B.: Regime classification of an exothermic reaction with nonuniform initial conditions. Combust. Flame **39**(2), 211–214 (1980). https://doi.org/10.1016/0010-2180(80)90017-6
15. Lee, J.H.S., Knystautas, R., Yoshikawa, N.: Photochemical initiation of gaseous detonations. AIAA **5**(11), 971–982 (1978). https://doi.org/10.1016/0094-5765(78)90003-6
16. Chaumeix, N., Imbert, B., Catoire, L., Paillard, C.E.: The onset of detonation behind shock waves of moderate intensity in gas phase. Combust. Sci. Technol. **186**(4–5), 607–620 (2014). https://doi.org/10.1080/00102202.2014.883259
17. Melguizo-Gavilanes, J., Bauwens, L.: A comparison between constant volume induction times and results from spatially resolved simulation of ignition behind reflected shocks: implications for shock tube experiments. Shock Waves **23**(3), 221–231 (2013). https://doi.org/10.1007/s00193-012-0403-x
18. Grogan, K.P., Ihme, M.: Regimes describing shock boundary layer interaction and ignition in shock tubes. Proc. Combust. Inst. **36**(2), 2927–2935 (2017). https://doi.org/10.1016/j.proci.2016.06.078
19. Lee, C.B., Wu, J.Z.: Transition in wall-bounded flows. Appl. Mech. Rev. **61**(3), 030802 (2008). https://doi.org/10.1115/1.2909605
20. Chen, Z., Burke, M.P., Ju, Y.: Effects of Lewis number and ignition energy on the determination of laminar flame speed using propagating spherical flames. Proc. Combust. Inst. **32**(1), 1253–1260 (2009). https://doi.org/10.1016/j.proci.2008.05.060
21. Chen, Z.: Effects of radiation and compression on propagating spherical flames of methane/air mixtures near the lean flammability limit. Combust. Flame **157**(12), 2267–2276 (2010). https://doi.org/10.1016/j.combustflame.2010.07.010
22. Dai, P., Chen, Z.: Supersonic reaction front propagation initiated by a hot spot in *n*-heptane/air mixture with multistage ignition. Combust. Flame **162**(11), 4183–4193 (2015). https://doi.org/10.1016/j.combustflame.2015.08.002
23. Kee, R., Rupley, F., Miller, J.: A Fortran program for modeling steady laminar one-dimensional premixed flames. Sandia National Laboratory Report SAND89-8009B (1989)
24. Kee, R., Grcar, J., Smooke, M., Miller, J.: CHEMKIN-II: a Fortran package for the analysis of gas-phase chemical kinetics. Sandia National Laboratory Report SAND85-8240 (1985)
25. Strang, G.: On the construction and comparison of difference schemes. SIAM J. Numer. Anal. **5**(3), 506–517 (1968). https://doi.org/10.1137/0705041
26. Toro, E.F.: Riemann solvers and numerical methods for fluid dynamics, 2nd edn. Springer, Berlin (1999). https://doi.org/10.1007/978-3-662-03915-1
27. Bussing, T.R.A., Murman, E.M.: Finite-volume method for the calculation of compressible chemically reacting flows. AIAA **26**(9), 1070–1078 (1985). https://doi.org/10.2514/3.10013
28. Chen, Z.: On the accuracy of laminar flame speeds measured from outwardly propagating spherical flames: methane/air at normal temperature and pressure. Combust. Flame **162**(6), 2442–2453 (2015). https://doi.org/10.1016/j.combustflame.2015.02.012
29. Yu, H., Chen, Z.: End-gas autoignition and detonation development in a closed chamber. Combust. Flame **162**(11), 4102–4111 (2015). https://doi.org/10.1016/j.combustflame.2015.08.018
30. Qi, C., Chen, Z.: Effects of temperature perturbation on direct detonation initiation. Proc. Combust. Inst. **36**(2), 2743–2751 (2017). https://doi.org/10.1016/j.proci.2016.06.093
31. Yu, H., Qi, C., Chen, Z.: Effects of flame propagation speed and chamber size on end-gas autoignition. Proc. Combust. Inst. **36**(3), 3533–3541 (2017). https://doi.org/10.1016/j.proci.2016.07.123
32. Faghih, M., Han, W., Chen, Z.: Effects of Soret diffusion on premixed flame propagation under engine-relevant conditions. Combust. Flame **194**, 175–179 (2018). https://doi.org/10.1016/j.combustflame.2018.04.031
33. Zhang, W., Faqih, M., Gou, X., Chen, Z.: Numerical study on the transient evolution of a premixed cool flame. Combust. Flame **187**, 129–136 (2018). https://doi.org/10.1016/j.combustflame.2017.09.009
34. Li, J., Zhao, Z., Andrei, K., Dryer, F.L.: An updated comprehensive kinetic model of hydrogen combustion. Int. J. Chem. Kinet. **36**(10), 566–575 (2004). https://doi.org/10.1002/kin.20026
35. Liu, S., Hewson, J.C., Chen, J.H., Pitsch, H.: Effects of strain rate on high-pressure nonpremixed *n*-heptane autoignition in counterflow. Combust. Flame **137**(3), 320–339 (2004). https://doi.org/10.1016/j.combustflame.2004.01.011
36. Sharpe, G.J., Short, M.: Ignition of thermally sensitive explosives between a contact surface and a shock. J. Phys. Fluids **19**(12), 126102 (2007). https://doi.org/10.1063/1.2821909
37. Basevich, V.Y., Lidskii, B.V., Frolov, S.M.: Mechanisms of the amplification of a shock wave passing through a cool flame zone. Russ. J. Phys. Chem. B **4**(1), 101–109 (2010). https://doi.org/10.1134/S1990793110010161

38. Gu, X.J., Emerson, D.R., Bradley, D.: Modes of reaction front propagation from hot spots. Combust. Flame **133**(1–2), 63–74 (2003). https://doi.org/10.1016/s0010-2180(02)00541-2
39. Liepmann, H.W., Roshko, A.: Elements of Gasdynamics. Dover Publications, NY (2002)
40. Zhao, Z.L., Chen, Z., Chen, S.Y.: Correlations for the ignition delay times of hydrogen/air mixtures. Chin. Sci. Bull. **56**(2), 215–221 (2011). https://doi.org/10.1007/s11434-010-4345-3
41. Petersen, E.L., Davidson, D.F., Hanson, R.K.: Ignition delay times of ram accelerator CH_4/O_2/diluent mixtures. J. Propuls. Power **15**(1), 82–91 (1999). https://doi.org/10.2514/2.5394
42. Petersen, E.L.: Interpreting endwall and sidewall measurements in shock-tube ignition studies. Combust. Sci. Technol. **181**(9), 1123–1144 (2009). https://doi.org/10.1080/00102200902973323